

Electro-osmotic properties of porous permeable films

Elena F. Silkina,¹ Naren Bag,² and Olga I. Vinogradova^{1,2,*}

¹*Frumkin Institute of Physical Chemistry and Electrochemistry,*

Russian Academy of Sciences, 31 Leninsky Prospect, 119071 Moscow, Russia

²*DWI - Leibniz Institute for Interactive Materials, Forckenbeckstr. 50, 52056 Aachen, Germany*

(Dated: March 18, 2020)

Permeable porous coatings on a flat solid support significantly impact its electrostatic and electrokinetic properties. Existing work has focused on simplified cases, such as weakly charged and/or thick porous films, with limited theoretical guidance. Here, we consider the general case of coatings of any given volume charge density and obtain analytic formulas for electrostatic potential profiles, valid for any film thickness and salt concentration. They allow us to calculate analytically the difference between potentials at solid support and at interface with an outer electrolyte, that is the key parameter ascertaining the functionality of permeable coatings. Our analysis provides a framework for interpreting and predicting specific for porous films super-properties, from an enhanced ion absorption to a giant amplification of electro-osmotic flows. The results are relevant for hydrogel and zeolite coatings, porous carbon and ion-exchange resins, polyelectrolyte brushes, and more.

Permeable for water and ions charged porous materials, such as cross-linked polyelectrolyte networks or hydrogels, ion-exchange resins, silica gels, zeolites, porous membranes and electrodes have found practical use in a large body of applications including water desalination [1], tissue engineering [2, 3], electrochemical systems [4], and more. Porous films, either thick or extremely thin (e.g. polyelectrolyte brushes [5]) can be formed on a wide variety of supports, providing properties, such as improved transport and storage capacities for ions, that they did not have when impermeable.

The quantitative understanding of novel equilibrium and transport properties, which could not be achieved without porosity and high intrinsic charge density is still challenging, even for planar coatings. Analytic solutions based on a linearized mean-field Poisson-Boltzmann theory are known for weakly charged porous films [6–8], but these results do not apply to highly charged coatings, where nonlinear electrostatic effects could become significant, leading to super-properties. The non-linear electrostatic problem has been treated using numeric and semi-analytic approaches [6, 9, 10], and some simple expressions have also been proposed for thick, compared to the Debye screening length λ_D , coatings [11, 12]. The results suggest relations between the Donnan, Ψ_D , and the surface, Ψ_s , potentials for thick and/or weakly charged films [6, 12], and that zeta-potential, which is the measure of electrokinetic mobility, generally exceeds Ψ_s [10, 13]. Nevertheless, general principles to control Ψ_s or electro-osmotic velocity have not yet been established in the case of high intrinsic charge of coatings, where the implication of porosity is the most pronounced.

In this letter, we develop a non-linear theory of electro-osmotic equilibria that describes analytically the distribution of a potential in the presence of a planar porous coating. Our model is valid even when the volume charge density is quite large, and can be used for any salt concentration and thickness of a porous layer. From this

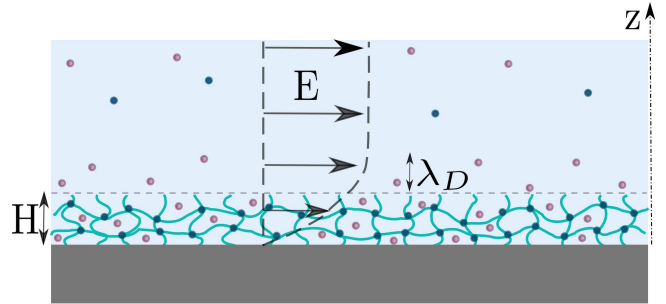


FIG. 1. Porous film of thickness H in contact with an electrolyte solution. The film is permeable for ions, so that the potential at the support, ψ_0 , and the surface potential, ψ_s , are established self-consistently. An outer electrostatic diffuse layer of a thickness, which is of the order of the Debye screening length, $\lambda_D \equiv \kappa^{-1}$, is formed in the vicinity of the porous coating. The application of a tangential electric field, E , leads to an electro-osmotic flow of a solvent (shown by arrows).

theory, we derive electrolyte concentration profiles that provide a framework for interpreting absorption properties and boosting storage capacities for ions. We also obtain an upper bound on an electro-osmotic velocity (that also constrains the attainable zeta-potential), and provide guidance for amplification of electro-osmotic flows.

The system geometry is shown in Fig. 1. The charged permeable film of a thickness H and a fixed volume charge density ϱ is placed in an 1:1 electrolyte solution of bulk concentration c_∞ and permittivity ε . Ions obey Boltzmann distribution, $c_\pm(z) = c_\infty \exp(\mp \psi(z))$, where $\psi(z) = e\Psi(z)/(k_B T)$ is the dimensionless electrostatic potential, e is the elementary positive charge, k_B is the Boltzmann constant, T is a temperature, and the upper (lower) sign corresponds to the positive (negative) ions. The inverse Debye screening length of an electrolyte solution, $\kappa \equiv \lambda_D^{-1}$, is defined as usually, $\kappa^2 = 8\pi\ell_B c_\infty$,

with the Bjerrum length $\ell_B = \frac{e^2}{\varepsilon k_B T}$. The problem we address are the profile of a cloud of counter-ions forming a diffuse electrostatic layer close to a planar surface of a film and the velocity of an electro-osmotic flow induced by an applied tangential electric field E .

We employ the classical nonlinear Poisson-Boltzmann theory [14], so that the profile $\psi(z)$ satisfies

$$\psi_{i,o}'' = \kappa^2 (\sinh \psi_{i,o} - \rho \Theta(H - z)), \quad (1)$$

where ' denotes d/dz , with the index $\{i, o\}$ standing for "in" ($z \leq H$) and "out" ($z \geq H$), $\rho = \frac{\varrho}{2ec_\infty}$, and the Heaviside step function $\Theta(z)$.

For an inner potential Eq.(1) can be formulated as

$$(\psi_i')' = 2\kappa^2 [\cosh \psi_i - \rho \psi_i], \quad (2)$$

Integrating Eq.(2) and using that $\psi_i'(0) = 0$ and $\psi_i(0) = \psi_0$, we get

$$\psi_i'^2 = 2\kappa^2 [\cosh \psi_i - \cosh \psi_0 - \rho(\psi_i - \psi_0)] \quad (3)$$

Integrating Eq.(1) in the outer region, and applying conditions $\psi_o' \rightarrow 0$ and $\psi_o \rightarrow 0$ at $z \rightarrow \infty$, we obtain

$$\psi_o'^2 = 2\kappa^2 [\cosh \psi_o - 1] \quad (4)$$

From Eq.(3) and Eq.(4) it follows that for planar films of any thickness ψ_0 and the surface potential, $\psi_s = \psi(H)$, are related as [12]

$$\psi_s \equiv \psi_0 - \frac{\cosh \psi_0 - 1}{\rho} \quad (5)$$

Further insight can be gained by recalling that $\cosh \psi$ represents a dimensionless local osmotic pressure of an electrolyte solution, $p = P/2c_\infty k_B T$, which takes its largest value of $p_0 = \cosh \psi_0$ at $z = 0$. Since $p(\infty) = 1$, Eq.(5) indicates that an excess osmotic pressure at the wall grows linearly with difference in potential, $\psi_0 - \psi_s$. It will be clear below that this is a main parameter that ascertains most of porous film properties.

Integrating Eq.(4) and using $\psi_o = \psi_s$ at $z = H$ we find that the ψ_o -profile is identical to derived for a single impenetrable wall [14]

$$\psi_o = 4 \operatorname{artanh} [\gamma e^{-\kappa(z-H)}] \quad (6)$$

where $\gamma = \tanh \frac{\psi_s}{4}$.

In the limit of $\kappa H \gg 1$, the inner region far from the interface may be modeled as electroneutral. Using Eq.(1) one can obtain the relation between $\psi_0 \equiv \psi_D$, where ψ_D is the Donnan potential, p_0 , and ρ

$$\psi_0 = \operatorname{arsinh}(\rho), p_0 = \sqrt{1 + \rho^2} \quad (7)$$

Then Eq.(5) can be transformed to

$$\psi_s = \psi_0 + \frac{1 - \sqrt{1 + \rho^2}}{\rho} \quad (8)$$

Using the symmetry arguments the exact expression for ψ_i could be constructed similarly to Eq. (6) as

$$\psi_0 - \psi_i = 4 \operatorname{artanh} [\gamma_i e^{-\kappa_i(H-z)}], \quad (9)$$

where κ_i is the inner screening length, which can be found as

$$\kappa_i = \kappa (\cosh \psi_0)^{1/2} \quad (10)$$

From Eq.(7) it then follows that $\kappa_i \simeq \kappa(1 + \rho^2)^{1/4}$, which indicates that when $\rho \ll 1$, a sensible approximation should be $\kappa_i \simeq \kappa$. However, when $\rho \gg 1$, $\kappa_i \simeq \kappa \sqrt{\rho}$, and the criterion of a thick film can be relaxed to $\kappa H \sqrt{\rho} \gg 1$. Besides κ_i , the value of $\psi_0 - \psi_i$ depends on γ_i . Using Eqs.(7) and (8) we obtain $\gamma_i = \tanh \left(\frac{\sqrt{1 + \rho^2} - 1}{4\rho} \right)$, which reduces to $\gamma_i \simeq \rho/8$ if $\rho \ll 1$, and $\gamma_i \simeq \frac{1}{4} \left(1 - \frac{1}{\rho} \right)$ when $\rho \gg 1$. This implies that γ_i is always smaller than 1/4. For such a small γ_i , the inner potential can be expanded about ψ_0 , and to first order in $\psi_0 - \psi_s$ we obtain

$$\psi_i(z) \simeq \psi_0 + (\psi_s - \psi_0) e^{\kappa_i(z-H)} \quad (11)$$

This equation has been derived before for weakly charged coatings [6]. We have now given a rigorous derivation justifying its validity for any inner and surface potentials.

Another limiting case of special interest is that of $\kappa H \ll 1$, where the asymptotic approach suggested before [15] can be employed. Expanding the potential in Eq.(1) about $z = 0$, we obtain, to second order in κz

$$\psi_i(z) \simeq \psi_0 - \frac{\rho}{2} (\kappa z)^2 \left[1 - \frac{\sinh \psi_0}{\rho} \right]. \quad (12)$$

From Eqs.(12) and (5) it follows that ψ_0 satisfies

$$\rho^2 - \rho \sinh \psi_0 - \frac{2(\cosh \psi_0 - 1)}{(\kappa H)^2} \simeq 0, \quad (13)$$

and standard manipulations then yield

$$\psi_0 \simeq \ln \left[\frac{2 + (\rho \kappa H)^2 + \rho \kappa H \sqrt{4 + (\kappa H)^2(1 + \rho^2)}}{2 + \rho(\kappa H)^2} \right] \quad (14)$$

When $\rho \gg 1$ this may be reexpressed as

$$\psi_0 \simeq 2 \operatorname{arsinh} \left(\frac{\rho \kappa H}{2} \right) - \ln \left(1 + \frac{\rho(\kappa H)^2}{2} \right). \quad (15)$$

For small $\rho \kappa H$, the ψ -profile is almost constant throughout the film,

$$\psi_0 \simeq \psi_s \simeq \rho \kappa H \quad (16)$$

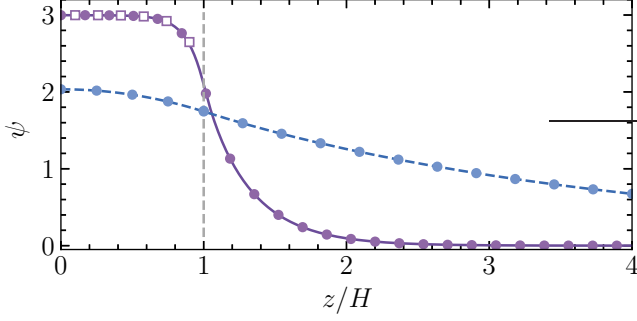


FIG. 2. A distribution of a potential built up by a film of $\rho = 10$, calculated numerically for $\kappa H = 0.3$ (dashed curve) and 3 (solid curve). Filled circles correspond to calculations from Eqs.(9) and (17), when $z/H \leq 1$, and from Eq.(6), when $z/H \geq 1$. Open squares are obtained from Eq.(11).

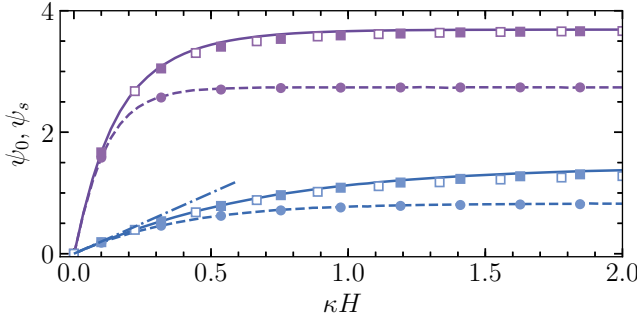


FIG. 3. Potentials at wall (solid lines) and surface (dashed) as a function of κH computed for fixed $\rho = 20$ (upper set of curves) and $\rho = 2$ (lower curves). Filled squares illustrate calculations from Eq.(14), circles are then obtained using Eq.(5). Open squares show results obtained using Eq.(15). Dash-dotted line is calculated from Eq.(16).

Finally, the inner ψ -profile of a thin film is given by

$$\psi_i(z) \simeq \psi_s - \frac{[\sinh \psi_0 - \rho]}{2} \kappa^2 (H^2 - z^2), \quad (17)$$

where ψ_0 and ψ_s are described by Eqs.(15) and (5).

In Fig. 2 we plot $\psi(z/H)$ computed for two different values of κH that are close to limits of thick and thin films, and a fixed ρ , corresponding to a situation of highly charged coatings. The form of the ψ -profile depends on κH . For $\kappa H = 3$ the inner potential shows a distinct plateau indicating that the intrinsic charge of the film is completely screened by electrolyte ions, i.e. global electroneutrality. The plateau potential is equal to ψ_D . However, when $\kappa H = 0.3$, there is no electroneutral region inside the film, and the potential at wall, ψ_0 , is much smaller than ψ_D . Also included in Fig. 2 are theoretical results obtained from Eqs.(5), (7), (14), and we conclude that in relevant areas they are in excellent agreement with numerical data.

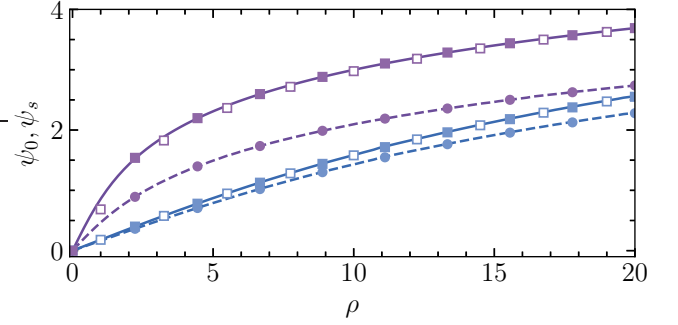


FIG. 4. Potentials at wall (solid lines) and surface (dashed) as a function of ρ computed for fixed $\kappa H = 3$ (upper set of curves) and $\kappa H = 0.2$ (lower curves). Filled squares illustrate calculations from Eq.(14), circles are then obtained using Eq.(5). Open squares show predictions of Eq.(15).

The startling conclusion from analysis of Eq.(13) is that it is also valid for sufficiently large κH . Indeed, in this case the last term on its left-hand side becomes very small in comparison with the first two, and ψ_0 is given by Eq.(7). It is tempting then to speculate that (14) will be applicable for any κH , and that a more elegant result, Eq.(15), can be used provided ρ is large enough. Clearly, Eq.(13) could become less accurate for intermediate κH , and it is of considerable interest to determine its regime of validity. To test this ansatz, numerical and theoretical ψ_0 and ψ_s have been calculated as a function of κH for different values of ρ . Specimen results are plotted in Fig. 3 confirming the validity of Eqs.(14) and (15) for all κH . As expected, Eq.(16), which can also be obtained using the linear theory [6], is valid only when $\rho \kappa H$ is very small and significantly overestimates potentials, which saturate at some κH , in other cases. The charge density dependence of ψ_0 and ψ_s is also of interest. Fig. 4 illustrates the weak growth of both potentials with ρ , and that $\psi_0 - \psi_s \simeq 1$ as $\rho \kappa H$ is increased. Finally, we again conclude that Eq.(14) fits accurately the numerical data. So does (15), except for $\rho \leq 1$, where some very small discrepancy is observed. Below we use compact Eq.(15) for all calculations, by omitting a discussion of the accuracy of our theory.

We make use of results presented above to predict and/or interpret some static and dynamic properties of porous films. One problem for which our analysis is relevant is the concentration of ions in an inner solution that is confined in porous media. Representative concentration profiles computed for highly charged porous films of $\rho = 10$ and two different values of κH are shown in Fig. 5. We see that in the inner region negative ions are significantly enriched, and positive are depleted. The degree of this enrichment and depletion depends on the values of ρ and κH . At the given ρ the degree of enrichment is ca.20 for a thick film of $\kappa H = 5$, but it is a few times smaller

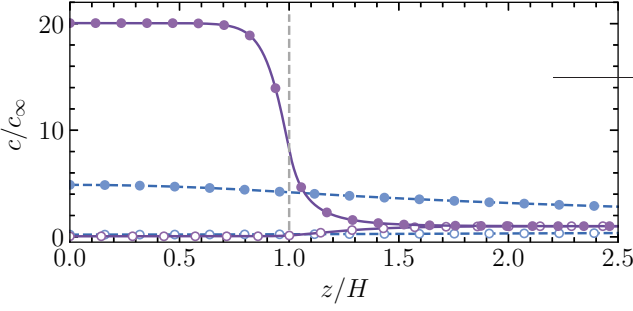


FIG. 5. Ion concentration profiles computed at $\rho = 10$ using $\kappa H = 0.2$ (dashed curves) and 5 (solid curves). Local concentrations of anions (filled circles) and cations (open circles) are calculated using Eqs.(6), (9), and (17).

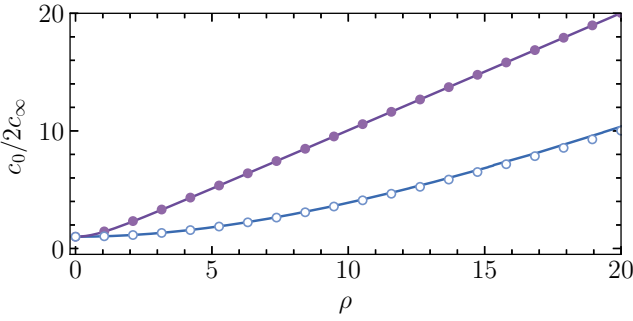


FIG. 6. Osmotic pressure at wall, $p_0 \equiv c_0/2c_\infty$, vs. ρ computed using $\kappa H = 3$ (upper curve) and 0.3 (lower curve). Filled and open circles are obtained from Eqs.(7) and (15).

when $kH = 0.2$. We also stress that for a chosen value of ρ their inner concentrations of cations practically vanish for both κH . To boost absorption of ions, coatings of larger ρ can be used, as illustrated in Fig. 6. Returning to Eq.(7), which describes perfectly numerical data for $\kappa H = 3$, it is clear that this curve corresponds to an upper attainable value of c_0 at given c_∞ . In other words, the absorption capacity cannot be further improved by making the coating thicker. However, the reduction in H could significantly reduce the concentration of adsorbed anions, especially at $\rho \leq 10$.

Another example for which our results are relevant is an electro-osmotic flow of a solvent of the dynamic viscosity η in an applied tangent electric field, E . We are now about to relate the dimensionless velocity, $v(z) = \frac{4\pi\ell_B\eta}{eE}V(z)$, of such a flow to ψ_0 and ψ_s . The liquid flow satisfies the generalized Stokes equation

$$v'' - \frac{v\Theta(H-z)}{\ell^2} = \psi'' + \kappa^2\rho\Theta(H-z), \quad (18)$$

with the Darcy-Brinkman correction for an inner flow, where ℓ is the Brinkman length. At the wall we ap-

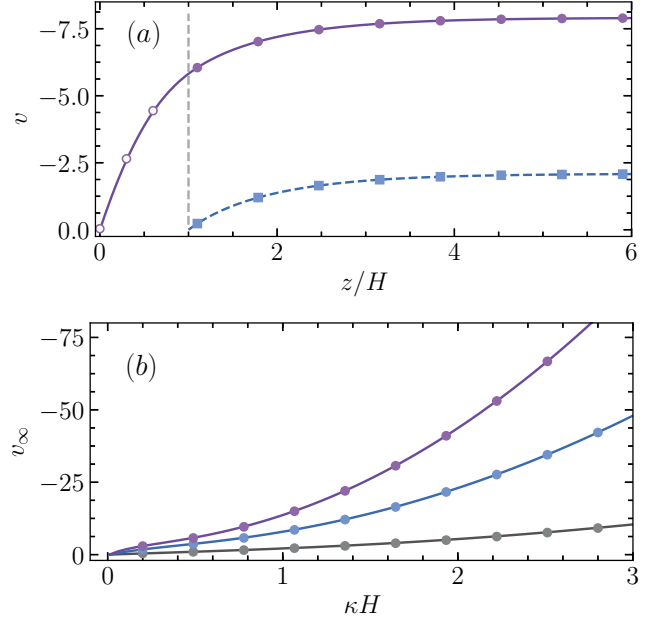


FIG. 7. (a) Bounds on electroosmotic velocity profile assuming $\ell/H \ll 1$ (dashed line) and $\ell/H \gg 1$ (solid line), respectively, computed for $\kappa H = 1$ and $\rho = 10$. Filled and open symbols indicate calculations from Eqs. (19) and Eq. (21). Squares are obtained using $v_s = 0$, circles correspond to $v_s = \psi_s + v_\infty$, where v_∞ is given by Eq. (22); (b) Computed upper bounds ($\ell/H \gg 1$) on v_∞ vs. κH (solid curves). From top to bottom $\rho = 20, 10$, and 2. Circles show results of calculations from Eq.(22).

ply a classical no-slip condition, $v_0 = v(0) = 0$, and far from the surface $v'_{z \rightarrow \infty} = 0$. To obtain bounds on the electro-osmotic velocity for arbitrary porous films with given ρ , we consider the limits of small flow extension into the porous medium, $\ell/H \ll 1$, and of $\ell/H \gg 1$, where an additional dissipation in the porous film can be neglected. These bounds constrain the attainable electroosmotic velocity and could provide theoretical guidance for porous film and electrolyte solution optimization. Note that from analysis of Eq.(18) it follows that the outer v -profile and velocity in the bulk are given by

$$v_o(z) = v_\infty + \psi_o(z), \quad v_\infty = v_s - \psi_s = -\zeta, \quad (19)$$

where ψ_o is defined by Eq.(6), $v_s = v(H)$ is the liquid velocity at surface, below we refer it to as slip velocity, and ζ is the normalized by $k_B T/e$ zeta potential. The problem, thus, reduces to calculation of v_s , with an upper attainable value ascertained by ℓ

$$v_s \simeq -\rho(\kappa H)^2 \left(\frac{\ell}{H} \right)^2 \simeq -\rho(\kappa\ell)^2, \quad (20)$$

that follows directly from Θ -terms of Eq.(18).

If we suppose $\ell/H \ll 1$, the slip velocity nearly vanishes, $\psi_s \simeq \zeta$, and $v_\infty \simeq -\psi_s$, which is equivalent to

the Smoluchowsky result. Fig. 7(a) includes numerical and theoretical v -profiles calculated for this case. Note that even for dense coatings the stagnant zone is at some distance from the surface [16] suggesting small finite v_s . With $\rho(\kappa H)^2 = 10$ used in Fig. 7(a) the largest possible v_s would be -0.1 , as follows from Eq.(20). In this example $\psi_s \simeq 2$, so that such a slip can be neglected. When $\ell/H \gg 1$, performing the integration of Eq.(18) twice, and imposing the continuity of v and v' at $z = H$, we find

$$v_i \simeq (\psi_i - \psi_0) - \rho\kappa^2 \left(Hz - \frac{z^2}{2} \right) \quad (21)$$

We recall that v_o is given by Eqs.(19) with

$$v_\infty \simeq -\psi_0 - \frac{\rho(\kappa H)^2}{2} \quad (22)$$

The v -profile for this case is also shown in Fig. 7(a). It turns out that even at moderate ρ and κH one can induce significantly enhanced, compared to the Smoluchowsky case, v_∞ , which is associated with the emergence of a large slip velocity, v_s . This implies that confined within the porous layer ions actively participate in the flow-driving mechanism by reacting to the field. The porous film acts as a charged immobile surface layer with absorbed mobile charges of the opposite sign, but note the difference from a known example of mobile surface charges at slippery wall [17]. In the latter case slippage is of a hydrodynamic origin and mobile surface charges induce a backward flow, reducing the amplification of electro-osmotic flow caused by hydrodynamic slip. By contrast, in the current work an inner solvent flow induces a forward flow and v_s itself. However, similarly to hydrophobic electrokinetics [17, 18], our large ζ no longer reflects the sole ψ_s . We now verify Eq.(22) and plot theoretical v_∞ vs. κH in Fig. 7(b) together with numerical data. Upon increasing κH at fixed ρ the amplitude of v_∞ grows nonlinearly, and in the case of $\rho \gg 1$ becomes several tens of times faster compared to a no-slip case, even at moderate κH . It is tempting to speculate that one can further amplify v_∞ making porous film thicker. However, when the film becomes thick enough, the condition $\ell/H \gg 1$ violates, and Eq.(22) is no longer valid.

Our simple analytic equations, obtained within mean-field nonlinear model, provide considerable insight into the electro-osmotic equilibria and flows in the presence of porous coatings. Many of our results will have validity beyond this particular geometry whilst others are certainly specific to it. The profiles of potentials are obviously generic - with the exception of small, compared to λ_D , objects. The same equilibria will occur for free-standing films, large objects of any geometry, and some general principles may be used to construct analogous expressions for thin curved objects as well.

Our rigorous bounds on the velocity of electro-osmotic flow are valid only for supported porous films, and can guide the design of coatings to amplify a variety of electrokinetic phenomena, including streaming current and diffusio-osmosis. Our work clarifies the nature of possible electro-osmotic flow enhancement and makes connection between Brinkman lengths and surface electrokinetic slip. The bounds we obtained constrain the attainable v_∞ , and it appears timely to derive expressions for an arbitrary ℓ/H , as well as to relate ℓ with the texture parameters of coatings.

We thank E.S.Asmolov for helpful discussions. This work was supported by the Ministry of Science and Higher Education of the Russian Federation and by the German Research Foundation (grant Vi 243/4-2) within the Priority Programme “Microswimmers - From Single Particle Motion to Collective Behaviour” (SPP 1726).

* Corresponding author: ovinograd@yahoo.com

- [1] S. Porada, L. Weinstein, R. Dash, A. van der Wal, M. Bryjak, Y. Gogotsi, and P. M. Biesheuvel, *ACS Appl. Mater. Interfaces* **4**, 1194 (2012).
- [2] D. F. Stamatialis, B. J. Papenburg, M. Gironas, S. Sainul, S. N. Bettahalli, S. Schmitmeier, and M. Wessling, *J. Membrane Sci.* **308**, 1 (2008).
- [3] H. H. Chung, M. Mireles, B. J. Kwarta, and T. R. Gaborski, *Lab on a Chip* **18**, 1671 (2018).
- [4] P. M. Biesheuvel, Y. Fu, and M. Z. Bazant, *Phys. Rev. E* **83**, 061507 (2011).
- [5] M. Ballauff and O. Borisov, *Current Opinion Colloid Interface Science* **11**, 316 (2006).
- [6] H. Ohshima and S. Ohki, *Biophys. J.* **47**, 673 (1985).
- [7] H. Ohshima and T. Kondo, *Biophys. Chem.* **38**, 117 (1990).
- [8] S. Chanda, S. Sinha, and S. Das, *Soft Matter* **10**, 7558 (2014).
- [9] J. F. Duval, *Langmuir* **21**, 3247 (2005).
- [10] G. Chen and S. Das, *J. Colloid Interface Sci.* **445**, 357 (2015).
- [11] H. Ohshima, *Sci. Technol. Adv. Mater.* **10**, 063001 (2009).
- [12] E. F. Silkin, T. Y. Molotilin, S. R. Maduar, and O. I. Vinogradova, *Soft Matter* **16**, 929 (2020).
- [13] V. D. Sobolev, A. N. Filippov, T. A. Vorob'eva, and I. P. Sergeeva, *Colloid J.* **79**, 677 (2017).
- [14] D. Andelman, *Handbook of biological physics* **1**, 603 (1995).
- [15] E. F. Silkin, E. S. Asmolov, and O. I. Vinogradova, *Phys. Chem. Chem. Phys.* **21**, 23036 (2019).
- [16] C. Kunert, J. Harting, and O. I. Vinogradova, *Phys. Rev. Lett.* **105**, 016001 (2010).
- [17] S. R. Maduar, A. V. Belyaev, V. Lobaskin, and O. I. Vinogradova, *Phys. Rev. Lett.* **114**, 118301 (2015).
- [18] L. Joly, C. Ybert, E. Trizac, and L. Bocquet, *Phys. Rev. Lett.* **93**, 257805 (2004).